SAND2000-1245C
RECEIVED
SEP 01 2000
OSTI

On the Feasibility of Fundamental-Mode Operation in Unstable-Resonator InGaN Lasers

W.W. Chow,[a] H. Amano[b] and I. Akasaki[b]

[a] Sandia National Laboratories, Albuquerque, NM 87185-0601, wwchow@somnet.sandia.gov
[b] Department of Materials Science and Engineering, High-Tech Research Center, Meijo University, 1-501 Shiogamaguchi Tempaku-ku, Nagoya 468-8502, Japan, amano@meijo-u.ac.jp

A wave-optical model that is coupled to a microscopic gain theory is used to explore solutions to the filamentation problem in group-III nitride quantum well lasers. A negative-branch unstable resonator is found to mitigate filament effects, enabling high-power fundamental-mode operation in broad-area lasers.

KEYWORD: Nitride quantum well lasers, high power, lateral or transverse modes, beam quality, unstable resonators, laser models.

1. Introduction

The short wavelength achievable in InGaN lasers is an advantage in applications such as digital versatile disk and laser printers. In order to fully utilize this advantage, high-power fundamental-mode operation is necessary. A limitation to fundamental-mode operation at high excitation is filamentation (or self-focusing) of the intracavity laser field in the semiconductor gain medium.[1] After the onset of filamentation, the overlap of the fundamental laser mode with the gain region is substantially reduced. The inversion that is undepleted by the fundamental mode becomes available to the higher order lateral modes, thereby increasing the likelihood of multimode operation. Filamentation also gives rise to high intracavity intensities, which increase the possibility of material damage.

In this paper, we use a wave-optical model to explore solutions to the filamentation problem in InGaN/GaN quantum well lasers. The gain medium is described with a microscopic theory.[2] The wave-optical laser model and the accompanying laser gain theory are described in Section 2. Section 3 introduces the concept of the antiguiding factor, which provides a measure of the strength of filamentation in a given quantum well structure. We show that the antiguiding factor in a nitride quantum well gain region may be significantly higher than those typical in other semiconductor lasers. There is also a strong dependence on quantum well width. Section 4 illustrates the effects of filamentation on the laser output in an optical resonator with plane facet mirrors. In Sec. 5, we propose a solution to the filamentation problem that involves unstable resonators.[3-6] A parametric study shows that a negative-branch unstable resonator is best suited for nitride quantum well lasers, in terms of maintaining single-mode operation at high excitation in broad-area lasers. The results of this paper are summarized in Sec. 6.

2. Theory

We adopt a coordinate system where y is the lateral (plane of quantum well) dimension, x is the transverse (perpendicular to quantum well plane) dimension, and z is along the resonator axis. The intracavity laser field is described by the sum of two-counter propagating waves,

$$E(\mathbf{r},t) = E_+(\mathbf{r},t) + E_-(\mathbf{r},t)\ , \qquad (1)$$

where we assume an electric field polarization in the plane of the quantum well. By assuming a weak lateral dependence in the effective refractive index, we write (in MKS units)

$$E_\pm(\mathbf{r},t) = \sqrt{\frac{1}{2\epsilon_0 cn}}u(x,y)v_\pm(y,z) \times e^{i(\pm Kz-\omega t)} + c.c.\ , \qquad (2)$$

where ϵ_0 and c are the permittivity and speed of light in vacuum, K and n are the laser wavevector and average refractive index in the host medium, and ω is the angular frequency. The transverse field distribution $u(x,y)$, which is a weak function of y, is determined by the epitaxial layers of the heterostructure. The lateral field distribution obeys the following equation, which is derived from Maxwell's equations:

$$\pm\frac{\partial v_\pm}{\partial z} = \Gamma\left[\frac{G(N)}{2} + iK_0\delta n_g(N)\right]v_\pm + \frac{i}{2K}\frac{\partial^2 v_\pm}{\partial y^2} - \alpha_{abs}v_\pm\ , \qquad (3)$$

where $K_0 = K/n$, Γ is the confinement factor, α_{abs} accounts for the internal optical losses, G is the local intensity gain, and δn_g is the carrier-induced refractive index change.

DISCLAIMER

This report was prepared as an account of work sponsored by an agency of the United States Government. Neither the United States Government nor any agency thereof, nor any of their employees, make any warranty, express or implied, or assumes any legal liability or responsibility for the accuracy, completeness, or usefulness of any information, apparatus, product, or process disclosed, or represents that its use would not infringe privately owned rights. Reference herein to any specific commercial product, process, or service by trade name, trademark, manufacturer, or otherwise does not necessarily constitute or imply its endorsement, recommendation, or favoring by the United States Government or any agency thereof. The views and opinions of authors expressed herein do not necessarily state or reflect those of the United States Government or any agency thereof.

DISCLAIMER

Portions of this document may be illegible in electronic image products. Images are produced from the best available original document.

In Eq. (3), $G(N)$ and $\delta n_g(N)$ at each location in the gain region are determined by

$$2K_0\delta n_g(N) + iG(N) = \frac{\omega}{\varepsilon_0 ncE}P(N)\,, \qquad (4)$$

where macroscopic polarization amplitude is

$$P(N) = \frac{2}{V}\sum_{\nu_e,\nu_h,\mathbf{k}} (\mu_{\mathbf{k}}^{\nu_e\nu_h})^* p_{\mathbf{k}}^{\nu_e\nu_h}(N)e^{i\omega t}\,, \qquad (5)$$

V is the active region volume, $\mathbf{k}$ is the carrier momentum in the quantum-well plane, $\nu_e(\nu_h)$ identifies the conduction (valence) quantum-well subband, $\mu_{\mathbf{k}}^{\nu_e,\nu_h}$ is the optical dipole matrix element, and $p_{\mathbf{k}}^{\nu_e,\nu_h}$ is the microscopic electric dipole moment due to an electron-hole pair. To calculate the microscopic dipole, we solve the semiconductor Bloch equations, assuming quasiequilibrium electron and hole populations.[2] These equations contain contributions from many-body interactions. Carrier-carrier correlations, giving rise to screening and dephasing, are treated at the level of quantum kinetic theory in the Markovian limit. The numerical solution of the semiconductor Bloch equations requires as input the electron and hole dispersions and the dipole matrix elements. We calculate these quantities using $\mathbf{k}\cdot\mathbf{p}$ theory and the envelope approximation for the wurtzite crystal symmetry. The effects of the screening of the quantum-confined Stark effect is taken into account by the iterative solution of the $\mathbf{k}\cdot\mathbf{p}$ Hamiltonian and Poisson equation.[8] Input parameters to the bandstructure calculations are the bulk material parameters. Table 1 of Ref. [8] gives the values for the alloy $In_{0.2}Ga_{0.8}N$ considered in this paper.

The carrier density N at each location in the gain region is determined by the steady state solution of the carrier density rate equation[7]

$$\frac{\partial N}{\partial t} = \frac{J(y)}{ed} - \gamma_{eff}N - \frac{G(N)}{2\hbar\omega}\left(|v_+|^2 + |v_-|^2\right)\,, \qquad (6)$$

where $J(y)$ is the injection current density, d is the sum of the quantum well widths, and γ_{eff} is an effective rate for carrier loss from spontaneous emission and nonradiative processes. The carrier density $N(y,z,t)$ in Eq. (6) is averaged over the transverse variation. The laser simulation involves the simultaneous solution of Eqs. (3) and (6), which are coupled via the gain G and the carrier-induced refractive index $\delta n_g(N)$ in Eq. (4).

3. Antiguiding Factor

Earlier studies involving near-infrared semiconductor lasers have shown the importance of the filamentation or self-focusing in a semiconductor gain medium on optical beam quality.[1] A useful measure of the filamentation strength is the antiguiding factor,

$$R = -2K_0\left(\frac{\partial\delta n_g}{\partial N}\right)\left(\frac{\partial G}{\partial N}\right)^{-1}\,. \qquad (7)$$

Using the semiconductor Bloch equations, we computed R at the gain peak as a function of peak gain G_{pk}. Two differences between the antiguiding factor of nitride lasers and that of other semiconductor lasers are shown in Fig. 1. First, the antiguiding factor in a nitride quantum well may be significantly higher. The 2 nm $Ga_{0.2}In_{0.8}N/GaN$ quantum well at a peak gain of $\approx 10^3\ cm^{-1}$ has $R > 6$, which is almost a factor of three higher than typical in near-infrared quantum-well lasers. A large antiguiding factor implies a greater likelihood for filamentation. A contribution to the high R is the high joined density of states because of the significantly heavier electron and hole effective masses in nitride compounds.

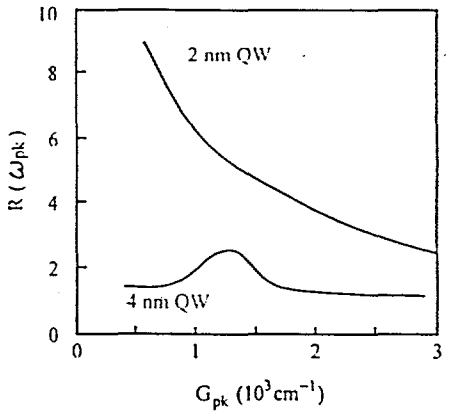

Fig. 1. Antiguiding factor at the gain peak for 2 nm and 4 nm $Ga_{0.2}In_{0.8}N/GaN$ quantum-well structures vs. peak gain.

The second difference is a stronger dependence of the antiguiding factor on quantum well width in the nitrides. Figure 1 shows a noticeably smaller R for the 4 nm $Ga_{0.2}In_{0.8}N/GaN$ quantum well. The reduction is due to contributions from the quantum-confined Stark effect on δn_g.[9] As in other semiconductor laser systems, the carrier-induced refractive index has a band filling contribution, which decreases δn_g with increasing carrier density. However, in a nitride quantum well there is also a contribution from the gradual screening of the quantum-confined Stark effect with increasing carrier density, which increases the dipole matrix element. Because δn_g is proportional to the square of the dipole matrix element,

this contribution counters that due to band filling. The cancellation is more complete in the wide 4 nm quantum well than the 2nm one because of the weaker quantum confinement in the former.

3. Filamentation

The effects of filamentation on nitride laser beam quality is depicted in Fig. 2. We assume a 10 μm stripe width, gain-guided laser operating with a 4 nm $Ga_{0.2}In_{0.8}N$/GaN quantum well gain region. The lateral field distribution has the form

$$v(y,z) = \sqrt{I(y,z)}\exp\left[-i\theta(y,z)\right] , \qquad (8)$$

where $I(y,z)$ and $\theta(y,z)$ are the laser field intensity and phase averaged over the transverse dimension of the gain region. Figure 2 shows $I(y,0)$ and $\theta(y,0)$ at different injection current, versus the lateral dimension y. The plane end facets are positioned at $z = 0$ and $z = L$, where the resonator length $L = 500$ μm. Other parameters used in the simulations are: confinement factor $\Gamma = 0.032$, facet reflectivities $R_1 = R_2 = 0.18$, and effective internal optical loss $\alpha_{abs} = 30$ cm^{-1}. For the present calculations, we ignore the effects of well width and composition variations in the InGaN quantum well gain region. For cluster dimensions that are smaller than the laser wavelength, these effects on optical propagation are negligible. However, the inhomogeneous broadening due to well width and composition variations will change the local gain and carrier-induced refractive index seen by the laser field, and these changes may be estimated by statistically averaging over the relevant fluctuations.[10]

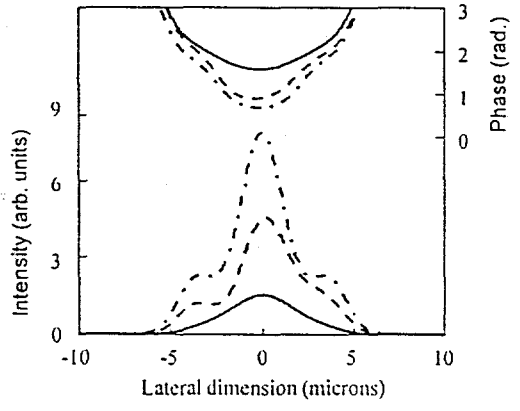

Fig. 2. Lateral intensity and phase distributions at output facet for 10 μm stripe width GaInN quantum well laser operating with plane facets. The excitation levels are $J/J_{th} = 1.2$ (solid curve), 1.6 (dashed curve) and 2.0 (dot-dashed curve).

For excitations $J/J_{th} \leq 1.2$, where J_{th} is the threshold current density, the lateral intensity distribution extends over the entire stripe width [solid curve in Fig. 2 (a)]. Antiguiding by the gain medium and diffraction give rise to a diverging wavefront. The dashed and dotted curves for $J/J_{th} = 1.6$ and 2.0 show the narrowing or filamentation of the lateral intensity distribution at higher excitations. These narrow intracavity field distributions do not make effective use of the available gain. Along with the beam narrowing is the appearance of structure in the phase front.

The noticeably narrower lateral intensity lobes are commonly referred to as filaments. They occur when the intracavity intensity is sufficiently high to cause spatial hole burning. Because the carrier-induced refractive index increases with decreasing carrier density, a waveguide is formed at the spatial hole. The channeling of the laser field by the waveguide leads to the burning of a deeper hole, which in turn further concentrates the laser intensity at the spatial hole (self-focusing).

For each gain structure, there is an asymptotic filament width that is independent of stripe width. This asymptotic filament width is approached at high excitation when the focusing due to the gain medium is balanced by diffraction. The asymptotic filament width for the 2 nm quantum well gain region is considerably smaller than for the 4 nm quantum well gain region ($w_{1/2} \approx 2$ μm versus 4 μm). To prevent beam breakup (i.e. multiple filaments in the output beam) at high excitations, one should use a stripe width that is close to the asymptotic filament width. For the 2 nm quantum-well active region, a single-lobe field distribution may be maintained far above threshold if the stripe width is reduced to 2 μm. For the 4 nm quantum-well laser, this stripe width may be increased to 4 μm.

5. Unstable Resonators

In this section, we explore the use of an unstable resonator[3] to improve modal properties. An unstable resonator is characterized by diverging wavefronts, which we hope will counter the focusing effects of filamentation. While unstable resonators have been used in near-infrared semiconductor lasers to produce high single-mode power,[11] there are concerns regarding their ability to counter the stronger filamentation tendency in a nitride gain medium.

Figure 3 addresses some of those concerns. Plotted are the output lateral field distributions at different excitations, for an unstable resonator, 4 nm $Ga_{0.2}In_{0.8}N$/GaN quantum well laser. We considered a negative-branch unstable resonator consisting of a plane mirror and a concave mirror of radius of curvature $\rho_2 = 400$ μm, separated by a resonator length of 500 μm. The stripe width is 10 μm, which is considerably wider than the asymptotic filament

width discussed in the previous section. To enhance the effects of the curved facet, we use high mirror reflectivities, $R_1 = R_2 = 0.8$. Assuming a confinement factor of $\Gamma = 0.034$, the material threshold gain is $G_{th} = 10^{10}$ cm^{-1}.

Figure 3 shows single-mode intensity distributions that extend over the entire gain region. The phase distribution is relatively smooth and independent of excitation. The calculated output power scales linearly with injection current density, and there is little change in the lateral mode shape for excitations beyond twice the lasing threshold. The importance of the concave mirror becomes evident when we repeated the calculations for a laser with 0.8 reflectivity, plane facet mirrors. That laser operates multimode for $J/J_{th} > 1.5$.

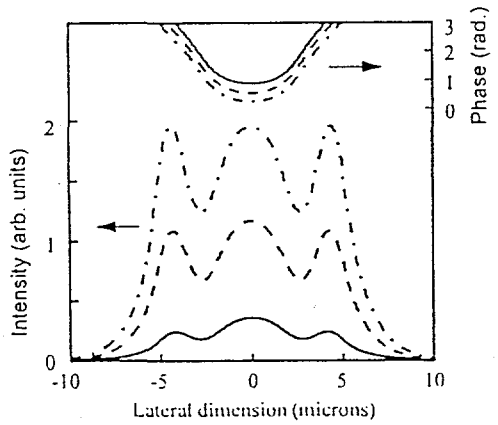

Fig. 3. Lateral intensity distribution at output facet for 10 μm stripe width GaInN quantum well laser operating with an unstable resonator. The excitation levels are $J/J_{th} = 1.1$ (solid curve), 1.5 (dashed curve) and 2.0 (dotted curve).

Comparison of Figs. 2 and 3 shows that while both lasers maintain single-mode operation up to twice the threshold current, the laser with the plane-plane resonator has a sharply peaked intensity distribution that can lead to material damage. Both lasers have relatively smooth phase distributions, where the significant aberrations involve only tilt and defocus, which are readily correctable with conventional optics. We computed the far-field intensity distributions for the lasers with these aberrations removed, and find that the intensity variations in the unstable resonator laser near-field do not result in noticeable degradation of the far field.

For the negative branch unstable resonator laser, a parametric study shows that the laser field distributions are relatively insensitive to concave mirror radius of curvature for the range 200 μm $\leq \rho_2 \leq$ 500 μm. The high magnification when $\rho_2 <$ 200 μm results in high lasing thresholds. For $\rho_2 >$ 500 μm, the resonator becomes stable, and single-mode operation is predicted for $J/J_{th} \leq 2$ and 500 μm $\leq \rho_2 \leq$ 4000 μm. However, the stable resonator modes have narrow lateral widths that are considerably smaller than the 10 μm wide gain region.

Because filamentation effects are stronger in nitride lasers than in other semiconductor lasers, the range of workable unstable resonators is more restrictive. For example, the curved facet must be highly reflective. We also find that a positive branch unstable resonator is not as effective in countering filamentation effects. Wide lateral intensity distributions that overlap reasonably well with the 10 μm wide gain region are obtained only with convex mirror curvature, $\rho_2 <$ 200 μm. The small radius of curvature leads to high laser threshold currents, and the resulting laser output is highly diverging, with most of the intensity concentrated in two off-axis peaks. In terms of sensitivity to the quantum well structure, the choice of unstable resonator configurations is quite restrictive for the 2 nm wide quantum well structure, where filamentation effects are significantly stronger than in the 4 nm quantum well case.

6. Conclusion

In summary, filamentation effects are generally stronger in nitride lasers than in other semiconductor lasers. Furthermore, there is a strong quantum-well width dependence because of the quantum-confined Stark effect. A wave-optical model that is coupled to a microscopic gain theory is used to explore solutions to the filamentation problem. We find that the intracavity beam spreading effects of an appropriately designed unstable resonator can balance filamentation effects, resulting in fundamental-mode operation in broad-area InGaN quantum well lasers at high excitations. For nitride lasers, negative-branch unstable resonators are preferable to the more commonly used positive-branch unstable resonators, in terms of sensitivity to mirror curvatures and reflectivities.

Acknowledgment

This work was supported in part by the U. S. Department of Energy under contract No. DE-AC04-94AL85000.

1) P. Kirkby, A. Goodwin, G. Thompson and P. Selway, IEEE J. Quantum Electron. **QE-13**, (1977) 705.
2) W. W. Chow and S. W. Koch, *Semiconductor-Laser Fundamentals: Physics of the Gain Materials* (Springer, Berlin, 1999).
3) A. E. Siegman, *Lasers* (University Science Books, Mill Valley, 1986).

4) A. P. Bogatove, P. G. Eliseev, M. A. Man'ko, G. T. Mikaelyan and Y. M. Popov, Sov. J. Quantum Electron. **10**, (1980) 620.
5) R. R. Craig, L. W. Casperson, O. M. Stafsudd, J. J. J. Yang, G. Evans and R. Davidheiser, Electron. Lett. **21** (1985) 62.
6) J. Salzman, T. Venkatesan, R. Lang, M. Mittelstein and A. Yariv, Appl. Phys. Lett. **46** (1985) 218.
7) W. W. Chow, S. W. Koch and M. Sargent III, *Semiconductor-Laser Physics* (Springer Verlag, Berlin, 1994), Chap. 10.
8) W. Chow, M. Kira and S. W. Koch, Phys. Rev. B **60** (1999) 1947.
9) W. W. Chow, H. Amano and I. Akasaki, Appl. Phys. Lett. **75** (2000) 1647.
10) W. W. Chow, A.F. Wright, A. Girndt, F. Jahnke and S. W. Koch, Appl. Phys. Lett. **71** (1997) 2608.
11) M. Tilton, G. Dente, A. H. Paxton, J. Cser, R. K. DeFreez, C. E. Moeller and D. Depatie, IEEE J. Quantum Electron. **QE-27** (1991) 2098.